Philosophical Magazine

ISSN: 1478-6435 (Print) 1478-6443 (Online) Journal homepage: http://www.tandfonline.com/loi/tphm20

A study of the determination of grain boundary diffusivity and energy through the thermally grown oxide ridges on a Fe-22Cr alloy surface

Yu Lin, David E. Laughlin & Jingxi Zhu

To cite this article: Yu Lin, David E. Laughlin & Jingxi Zhu (2016): A study of the determination of grain boundary diffusivity and energy through the thermally grown oxide ridges on a Fe-22Cr alloy surface, Philosophical Magazine

To link to this article: http://dx.doi.org/10.1080/14786435.2016.1263403

Published online: 27 Dec 2016.

PHILOSOPHICAL MAGAZINE, 2016
http://dx.doi.org/10.1080/14786435.2016.1263403

Taylor & Francis
Taylor & Francis Group

A study of the determination of grain boundary diffusivity and energy through the thermally grown oxide ridges on a Fe-22Cr alloy surface

Yu Lin[a], David E. Laughlin[a,b] and Jingxi Zhu[c,d]

[a]Department of Materials Science and Engineering, Carnegie Mellon University, Pittsburgh, PA, USA; [b]ALCOA Professor of Physical Metallurgy, Pittsburgh, PA, USA; [c]School of Electronics and Information Technology, Sun Yat-sen University–Carnegie Mellon University Joint Institute of Engineering, Sun-Yat Sen University, Guangzhou, China; [d]Sun Yat-sen Univeristy–Carnegie Mellon University Shunde International Joint Research Institute, Foshan, China

ABSTRACT

The grain boundaries (GBs) present in polycrystalline materials are important with respect to materials behaviour and properties. During the transient stage of oxidation, the higher GB diffusivity results in heterogeneous oxidation structures in the form of oxide ridges that emerge along the alloy GBs. In an attempt to delve into the more fundamental aspects of the GBs, such as GB energy, the size of the oxide ridges was quantitatively measured by atomic force microscopy on the post oxidation surface of a Fe-22 wt % Cr alloy after an oxidation exposure at 800 °C in dry air. The GB diffusivity was calculated utilising the ridge size data and the relationship between the GB diffusivity and the GB characteristics was determined. Furthermore, the GB energy was calculated from the GB diffusivity data, also to make comparison with the data available in the literature. The absolute value of the calculated GB energy was quite close to the values reported in the literature. However, compared to the extremely low temperature (0 K) data-set from the literature, the data-set obtained from this study showed much less spread. The smaller variation range may be attributed to the higher temperature condition (1073 K) in this study.

ARTICLE HISTORY
Received 7 July 2016
Accepted 16 November 2016

KEYWORDS
Grain boundary; high temperature oxidation; grain boundary diffusion; grain boundary energy

1. Introduction

Grain boundaries (GB) are the most important interfaces in polycrystalline materials, whose state and nature are one of the most defining factors in the materials behaviours and properties, whether the materials serve as structural components or are placed in corrosive environment. Because of the importance of GBs, researchers are still in pursuit of furthering the fundamental understanding of the correlation between the aforementioned phenomena and the GB characteristics.

In the context of high temperature, degradation of metallic materials, because of the presence of sheer amount of GB interfaces, GB interfacial transport and/or GB motion are

CONTACT Yu Lin yulin1@andrew.cmu.edu; Jingxi Zhu zhjingxi@mail.sysu.edu.cn

usually important. Alloy GBs are well known as short circuit diffusion paths and the GB diffusivities of the metal elements in the alloy have been found to be directly related to the GB structure characteristics, resulting in heterogeneities in oxidation/corrosion rates and structures [1–4].

Examples of this can be found in the Fe–Cr-based alloys that are widely used in various high-temperature applications for their cost-effectiveness compared to Ni-based alloys. When oxidised, selective oxidation of Cr takes place due to its higher affinity to oxygen than Fe and the resulting chromium oxide can provide some protection against further fast oxidation of the alloy. Due to the fast diffusion through alloys GBs, especially during the very early stages of oxidation, heterogeneous oxidation structures such as ridges of oxides have been observed to emerge from the GB traces, as reported in Refs. [5,6]. The morphology of such oxide ridges can be seen in Figure 1, which outlining the alloy grains beneath the scale layer. Moreover, the nature of these initial oxides formed in the transient stage can influence the subsequent scaling behaviour and the nature of the scale well into the steady-state oxidation [7,8].

It is known that the diffusivity of a GB depends greatly on the GB characteristics, which includes the GB misorientation (the misorientation axis and the misorientation angle) and the orientation of the GB plane [3,9–11]. Turnbull and Hoffmann developed a linear relationship between the GB diffusion product and the misorientation angle for low-angle GBs [12]. Moreover, several measurements of the GB diffusivity–misorientation angle curves have revealed the presence of cusps at misorientations corresponding to coincident site lattice (CSL) GBs [13–16]. Thorning and Sridhar studied the oxide growth on TRIP steel surface during the transient stage [6]. They found that there was a clear difference in the formation kinetics and post oxidation morphology of the ridges at different GB traces: The ridges tended to evolve homogenously on the straight GB traces and heterogeneously on the curved GB traces. This phenomenon was a strong evidence for the direct relationship between oxide ridge evolution and the underlying GB characteristics in TRIP steels.

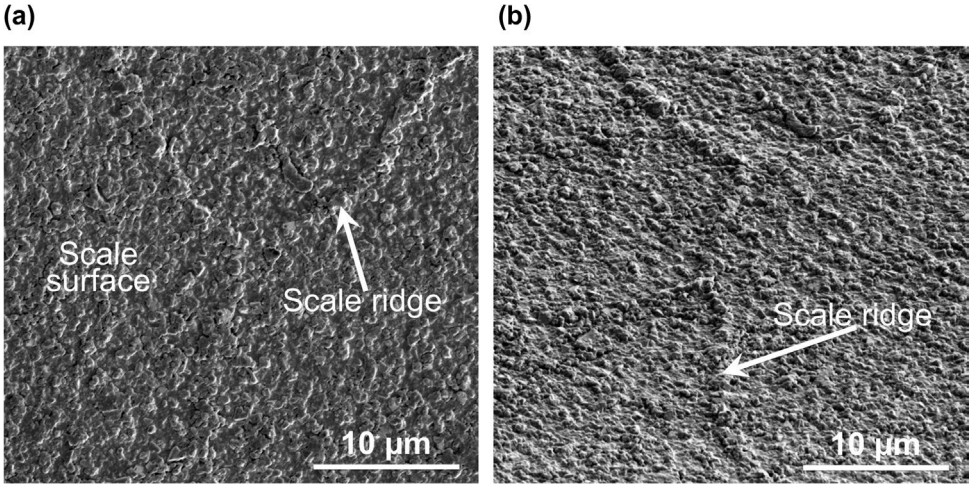

Figure 1. Scanning electron microscopy images of scale ridges after 15 min of exposure in dry air at 800 °C: (a) planeview micrograph, (b) view at 52° stage tilt.

The GB energy has a similar dependence on GB misorientation as the GB diffusivity. Attempts have been made to relate the GB energy to the GB diffusivity. The Borisov model which describes this relationship was proposed in the 1960s and is still widely utilised [17].

In a previous work, Zhu et al. [1] studied a large number of initial scale ridges grown on a Fe-22Cr alloy at 800 °C, with regard to the GB diffusivity and the GB misorientation in a qualitative but semi-statistical manner. The current study is a continuation of this study, by considering more fundamental aspects of the GBs, and has been carried out as follows:

- Quantitative measurement of the ridge size was performed first, to validate the relationship established in the previous qualitative study.
- Assuming the volume of the oxide ridges is an accurate representation of the diffusivity of the underlying alloy GBs, the GB diffusion coefficient was calculated for each of the individual GB segments.
- From the GB diffusion coefficients, the GB energy data were extracted and compared to the data available in the literature.

2. Experimental

2.1. Ridge size measurement

The sample used for this experiment was prepared, processed and characterised in a previous study and the experimental details on the sample preparation can be found in [1]. In order to quantify the ridge size, maps of the heights of the ridges were obtained by atomic force microscopy (AFM). Since it was not practical to extract the individual segmental oxide volume for a statistically representative number of ridges, the cross-sectional areas of the ridges were extracted instead for approximation. Figure 2 shows the general methodology for the quantification of the ridge size. First, a height map was collected from the mid-section of a ridge between two GB triple junctions (Figure 2(a)) with AFM. Then, 10 surface height profiles of the ridge and the oxides grown in the two neighbouring grains were plotted (shown as the horizontal line in the AFM height map). For each profile, a baseline was determined for both left and right sides of the ridge and subsequently averaged

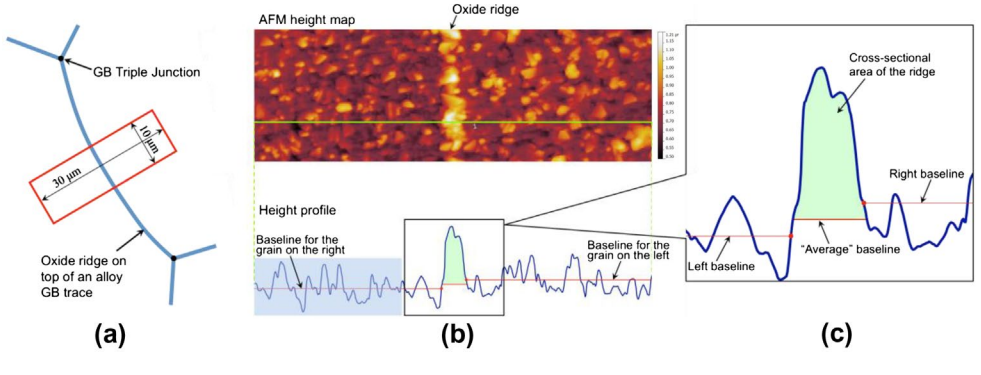

Figure 2. (colour online) Data collection and processing: (a) AFM height map collection. (b) Example of a height map and plotting a height profile of the ridge from the map. (c) Processing of the ridge profile and the determination of the cross-sectional area of the ridge.

(Figure 2(b)). The area above the 'average' baseline was taken as the cross-sectional area of the ridge (Figure 2(c)). Finally, the cross-sectional areas calculated from each profile were averaged and taken as the size of that particular ridge.

The AFM topography images of the post oxidation sample were acquired using the Solver Next scanning probe system and NanoWorld PNP-TR probes, in contact error mode. High-resolution and careful image corrections were performed to ensure accurate height maps [18,19]. The data collection procedures are shown in Figure 3. During the scan, the optical microscope image of the ridge under the AFM was compared to the surface EBSD map (Figure 3(a)) taken before oxidation to obtain the characteristics of corresponding alloy GB. For each ridge, a rectangle area of 30 × 10 μm at the midpoints between two triple junctions was selected to avoid the areas near triple junctions. The lateral resolution of the maps was 15 nm. Image Analysis P9 and Gwyddion softwares were used to process all the maps. A second order correction was applied to correct the map inclination and distortion. The image was further corrected using the error signal map.

Because AFM can only measure the part of the cross-sectional area of the ridge that protruded out of the baseline scale surface, (the area filled with oblique lines in Figure 4), the area under the baseline was later added by calculating the area of the rectangle filled with horizontal lines. This was done using the average oxide thickness in grain interiors as the width (see Figure 4), i.e. the average oxide thickness of the scale everywhere else on the sample surface except locations with ridges, which was determined from cross-sectional SEM images. Despite the possible error involved in averaging the oxide thickness, ridge cross-sectional areas obtained this way should reflect closely the diffusivity of the GB beneath the ridge.

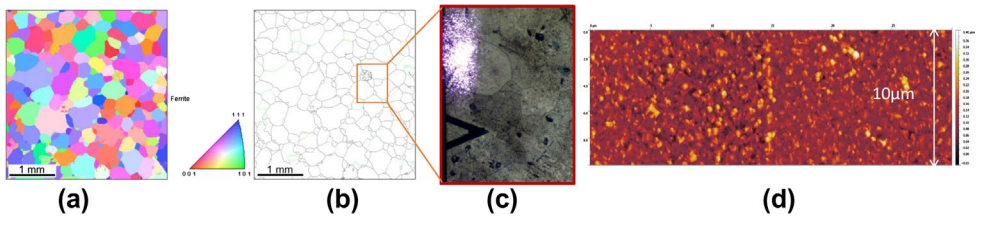

Figure 3. (colour online) Data collecting procedures: (a) EBSD map of the polycrystalline alloy surface and the inverse pole figure of ferrite. (b) Reconstructed GB map, in which green indicates disorientation angle <15° while black indicates disorientation angle >15°. (c) Optical microscope image taken under AFM while scanning, which corresponds to the region in the red rectangle in the reconstructed GB map. (d) AFM height map collected.

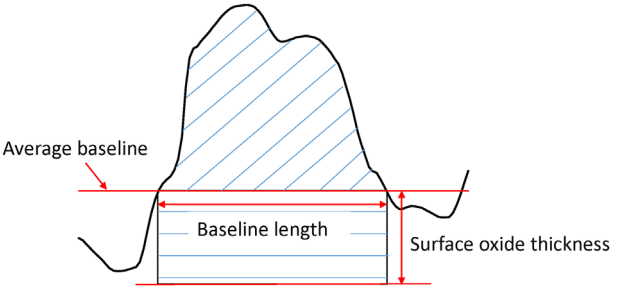

Figure 4. (colour online) Schematic drawing of the ridge cross-sectional area quantification.

2.2. Calculation of GB diffusivity

The measured ridge cross-sectional area was used to back-calculate the GB diffusivity of Cr. The simplified geometric model is shown in Figure 5. The assumptions made in this model include: (1) the oxidation process occurred at the free surface of the oxide; (2) the rate-limiting factor of oxidation was the diffusion of Cr along GBs [6]; and (3) the oxide scale was quite thin at this stage such that the stresses developed within it did not affect the oxidation process. The Cr diffusivity was calculated utilising two approaches. The first approach was based on the hypothesis that the amount of Cr in the oxide ridges normalised by the GB surface area should be equal to the integration of the Cr concentration profile in the alloy. The second approach was based on the hypothesis that the amount of Cr in the oxide ridges normalised by the GB surface area should be equal to the GB flux of Cr integrated by the total oxidation time, which should follow Fick's Law of diffusion.

As for the constituents of the oxide ridges, it was reported that the initial oxidation product of high manganese stainless steel (0.38 wt % and 0.9 wt % Mn) consisted of spinel ($Mn_xCr_{3-x}O_4$) and corundum (Cr_2O_3) [20]. Based on experimental observations, it was assumed here that half of the volume of the ridge was spinel and the other half was corundum. Also, the x in the spinel formula $Mn_xCr_{3-x}O_4$ was approximated as one. Therefore, the amount of Cr (in mole) per unit area (Q) accumulated on the surface along GBs during oxidation can then be expressed by Equation (1):

$$Q = \frac{2\left(\frac{1}{2}Al\right)\frac{\rho_{Cr_2O_3}}{M_{Cr_2O_3}}}{\delta l} + \frac{(3-1)\left(\frac{1}{2}Al\right)\frac{\rho_{MnCr_2O_4}}{M_{MnCr_2O_4}}}{\delta l} \tag{1}$$

where A is the ridge cross-sectional area determined with AFM data; l is the unit length of the GB segment; δ is the GB width; $\rho_{Cr_2O_3}$ is the density of Cr_2O_3 (5.2 g/cm^3); $M_{Cr_2O_3}$ is the molar mass of Cr_2O_3 (122 g/mol); $M_{MnCr_2O_4}$ is the molar mass of the spinel (223 g/mol) and $\rho_{MnCr_2O_4}$ is the density of the spinel, which can be calculated using the parameters in [21] and the result here was 4.9 g/cm^3.

The amount of Cr (in moles) per unit GB area should also equal the integration of the Cr concentration profile in the alloy. To solve for the Cr concentration profile, the Whipple

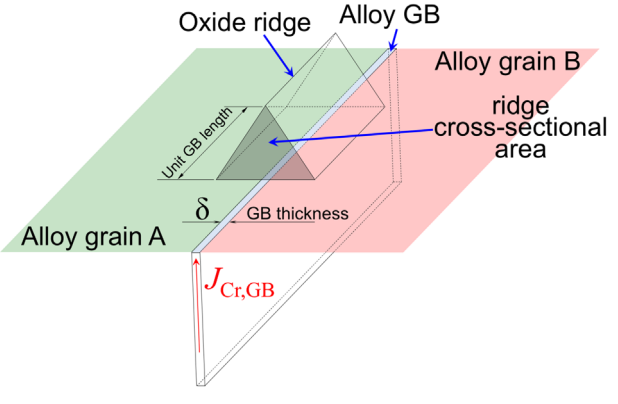

Figure 5. (colour online) Schematic drawing of the oxide ridge and the parameters for Cr GB diffusion coefficient calculation.

solution for the diffusion from a constant source of the isolated boundary model, first proposed by Fisher [22], was considered. However, because the exact solution was not convenient when evaluating the GB diffusion data, Kaur et al. [3] divided the GB diffusion regime B further into regimes B_1, B_2, B_3 and B_4 to simplify the exact solution into forms for practical applications. Here, we utilised the expression derived for the amount of diffusant penetrated through a unit area of the surface for the B_2 Regime, which is expressed as Equation (2):

$$Q = \frac{(22\% - 0)\frac{\rho_{\text{steel}}}{M_{\text{Cr}}} D^{1/4} t_0^{3/4} (2s\delta D_{\text{GB}})^{1/2}}{\delta \Gamma\left(\frac{7}{4}\right)} \tag{2}$$

where D is the Cr bulk diffusion coefficient; D_{GB} is the Cr diffusion coefficient through GBs; s is the segregation coefficient indicating the solute enrichment of the GB with respect to the matrix (approximated to 1 according to [23]); t_0 is the oxidation time (900 s); ρ_{steel} is the density of Crofer22 steel (7.7 g/cm^3); and M_{Cr} is the molar mass of Cr (52 g/mol). It was worth noting that the grain size term in the denominator in the original equation in Ref. [3] was replaced by GB width δ in this calculation since the Q calculated from Equation (1) was the amount of Cr accumulated on per unit GB surface area rather than per unit surface area.

On the other hand, the amount of Cr (in moles) per unit area should equal that of the integrated flux of Cr through GBs to the surface during oxidation, following Fick's law. In this case, we simplified the Cr GB diffusion into one that followed Fick's first law. The particularly large alloy grains of this sample and a short oxidation time allowed us to assume that the GB diffusion considered occurred among a monolayer of grains that made up the alloy surface. This could also be validated with estimated diffusion length, i.e. $(Dt)^{1/2}$, which was smaller than the average grain size, i.e. 0.182 mm. The concentration gradient along the GB of Cr was approximated as 22 wt % divided by the diffusion length. Thus, Q is expressed as Equation (3):

$$Q = \int_0^{t_0} D_{\text{GB}} \frac{(22\% - 0)\frac{\rho_{\text{steel}}}{M_{\text{Cr}}}}{\frac{(s\delta D_{\text{GB}})^{1/2}}{(4D/t)^{1/4}}} \mathrm{d}t \tag{3}$$

where the $\frac{(\delta D_{\text{GB}})^{1/2}}{(4D/t)^{1/4}}$ term is the GB diffusion length for the B regime [3].

By equating Equation (1) and Equation (2) and equating Equation (1) and Equation (3) and solving for the GB diffusion triple product, the expression of GB diffusivity of Cr in terms of ridge cross-sectional area was obtained for each individual GB segment.

2.3. Relating GB diffusion to GB energy

Once the GB diffusion coefficient was obtained for each of the individual GB segments, the GB energy could be calculated. A first approximation equation by Borisov et al. [17] was used for this calculation and expressed as Equation (4):

$$E = \frac{(kT)}{(\alpha a^2)} m \left[\left(\ln \frac{s\delta\theta}{a\lambda^{\alpha}} - \ln m\right)\right] \tag{4}$$

where E is the GB free energy; k is the Boltzmann constant; T is the temperature; m is the number of atomic layers forming the boundary (approximated as one by Borisov [17]); a is the mean distance between the equilibrium positions of the atoms (which was taken to be the lattice parameter 2.87 A); s is the segregation coefficient indicating the solute enrichment of the GB with respect to the matrix; δ is the width of the grain boundary; λ is related to the normal frequencies and the potential energies of the equilibrium and activated states (approximated as one according to Borisov [17]); the exponent α is equal to 1 if diffusion mechanism is predominately an interstitial one and α is equal to 2 if diffusion mechanism is a vacancy one (we assumed α is 2 here according to Ref. [3]); θ is the relative diffusion mobility, defined as the ratio of GB and lattice diffusion coefficient. The volume diffusivity of Cr in Fe at 800 °C was taken as 5.5×10^{-16} m^2/s [24]. The original Borisov's model was developed for pure metals. Later, Guiraldenq [25,26] modified this model so that it could be applied for hetero-diffusion of alloying atoms with properties similar to matrix atoms, which is the case of this study. Substituting in all the parameters and the expression of the GB diffusion coefficient, the GB free energy was obtained.

3. Results and discussion

3.1. Quantitative results of the oxide ridge sizes

The oxide ridge sizes which was measured quantitatively with AFM were plotted in Figure 6: the oxide ridge cross-sectional areas were averaged with 1° binning of the underlying GB disorientation angles, and then plotted as a function of GB disorientation angle. It was worth noting that disorientation was used to describe the GB misorientation in this study. For GBs with disorientation angles smaller than 10°, the ridge sizes were so small that it became very difficult to locate the ridges under the optics of the AFM. Thus, the data for GBs with disorientation angles less than 10° are not included. From 10° to about 25°, increasing the GB disorientation angle increased the ridge cross-sectional area significantly. The ridge cross sectional area remained almost constant with disorientation angle larger than 25° and dropped around 60°. This overall trend was quite consistent with the previous work [1].

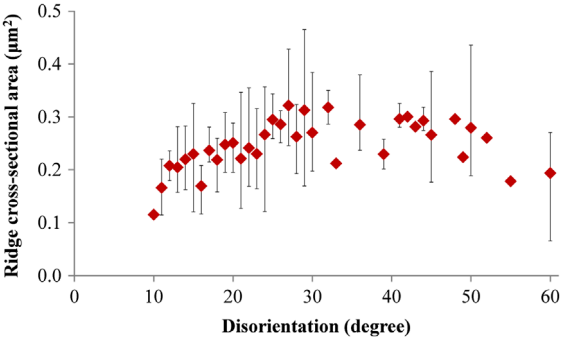

Figure 6. (colour online) Ridge cross-sectional area variation as a function of the disorientation angle of the alloy GBs beneath with error bars representing the ridge cross-sectional area variation range for each disorientation.

3.2. GB diffusivity

The calculated GB diffusivity of Cr using ridge cross-sectional area data utilising two approaches were plotted as a function of the disorientation angle in comparison with measured Cr diffusivity in pure Fe [24], Fe–Cr alloy [27–29] and Fe–Cr–Ni alloy [30,31] GBs reported in the literature, as shown in Figure 7. Compared with the reported Cr diffusivity, the calculation result in this study was slightly small but still within the variation range in the literature. One possible reason for this underestimation of GB diffusivity is that the oxide layer formed on grain interior region was not included in the estimation of Q in Equation (1). In addition, we could have underestimated the overall amount of Cr in the ridge with the assumptions on the spinel-corundum ratio. On the other hand, there are some factors which could have resulted in the overestimation of GB diffusivity, such as assuming the ridge was continuous (the ridges were actually formed by oxide nodules and were not continuous microscopically), approximating the Cr activity in the alloy to the concentration (which should be 0.48 according to calculation using FactSage software). Nevertheless, as will be addressed in the next section, such difference in diffusion coefficients becomes less important when the GB energy data are calculated.

For low angle GBs (below about 15°), Turnbull and Hoffmann developed a linear relationship between GB diffusion product and the misorientation angle using the spaced parallel dislocations model for tilt boundaries. As the disorientation angle increased, the spacing between the dislocation pipes became smaller and the cores of the dislocations gradually overlapped with each other. As a result, the boundary turns into a continuous slab of 'bad material' [32] and the dislocation pipe model fails to be valid [3]. Because of this disordered structure, the activation energy for elemental diffusion in high angle GBs is typically lower and hence their diffusivity was correspondingly higher [32]. On the other hand, the GB width was also larger for high angle GBs, but the effect was not as predominant as the exponential factor. This explains the fact that the GB diffusivity increased significantly from 10° to 25°.

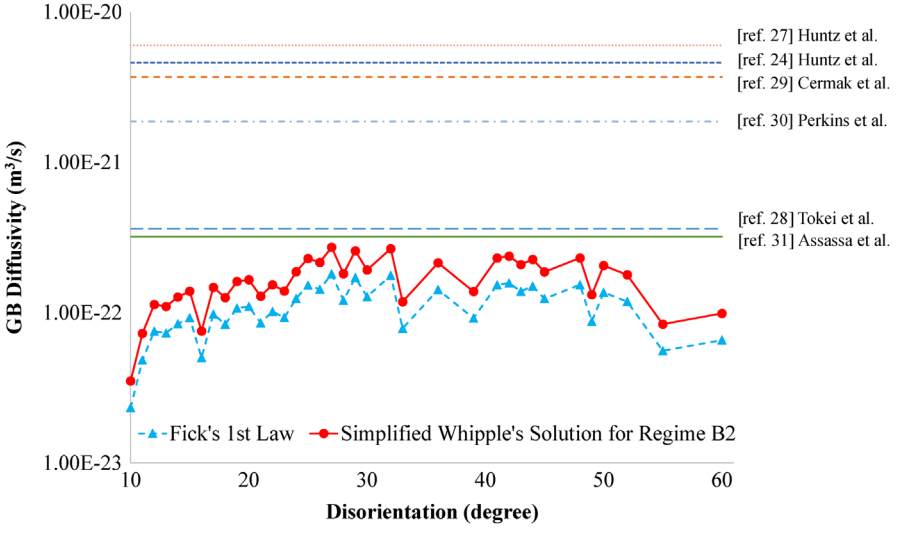

Figure 7. (colour online) Calculated GB diffusivity variation utilizing two approaches as a function of the disorientation angle of the alloy GBs, in comparison with data available in the literature [24,27–31].

The GB diffusivity was quite low for CSL GBs (only the data for Σ3 at 60° was collected in this work). The low diffusivity of CSL GBs can be interpreted by their more ordered structure and thus higher diffusion activation energy. The low elemental diffusivity in CSL GBs has attracted a number of investigations. Aleshin et al. studied the diffusion of Zn in ⟨0 0 1⟩ and ⟨1 1 1⟩ tilt boundaries in aluminium [13,14]. Their results revealed the presence of several activation energy maxima at CSL misorientation angles. The activation energy peaks at CSL misorientation angles were verified by Straumal et al. for the diffusion of In along Sn/Ge interphase ⟨0 0 1⟩ twist boundaries [15]. Budke et al. found a cusp of GB diffusion product at Σ5 GB misorientation angle in their study of diffusion of Au and Cu along [0 0 1] tilt boundaries in Cu [16]. Large GB plane inclination could result in higher diffusivity along CSL GBs, but that higher diffusivity is still lower than non-special GBs [33].

3.3. GB energy

The calculated GB energies are plotted as a function of disorientation angle in Figure 8. For comparison, the simulation results of Ratanaphan [34] are also shown in Figure 8. The absolute values of the data-set in [34] are in the range between 0.7 and 1.4 J/m^2, while the values of the data-sets in this study are in the range between 0.4 and 0.7 J/m^2. The factors which could have resulted in the underestimation of GB energy in calculation were mentioned in the previous section. In addition, another possible reason for the lower absolute values in this study is that the calculation in [34] was in pure Fe while the measurement in this study is in Fe alloy and hence impurity segregation effect should be taken into account. It should be noted, though, that the data-set in [34] was evaluated for 0 K, and in general, GB energy decreases with increasing temperature for pure metal while increases with increasing temperature for alloy [35]. The overall trends of the three data-sets are quite similar: The GBs with small disorientation angles have relatively low energies; as GB disorientation angle increased, the GB energy increased significantly and remained almost constant with disorientation angle larger than approximately 25°. However, compared to the extremely low

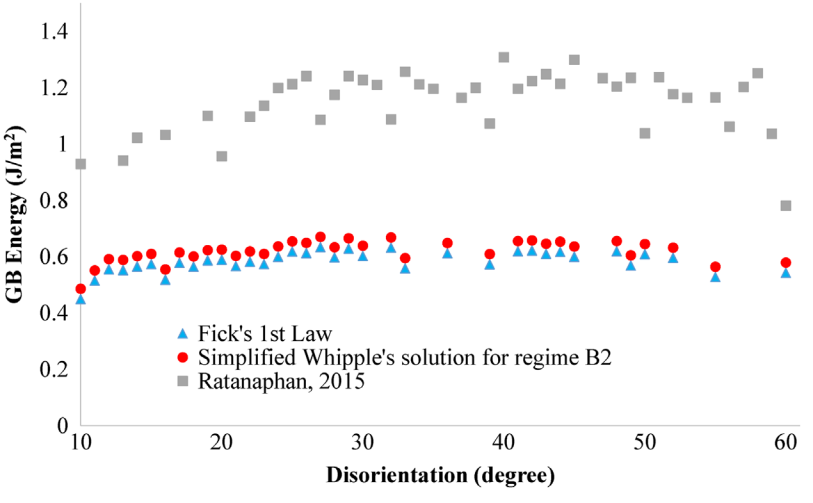

Figure 8. (colour online) Calculated GB energy variation utilizing two approaches as a function of disorientation angle, in comparison with the simulation of Ratanaphan et al. [34].

temperature data-set from Ref. [34], the data-sets obtained from this study showed much less spread. The difference between the max and min of the data-set from Ref. [34] was approximately 0.53 J/m^2, while that of the two data-sets from this study are both 0.18 J/m^2.

One explanation for the narrower variation range of the data-sets from this study is that the GB energy calculated in Ref. [34] was in pure Fe while the values obtained in this study was in a Fe alloy similar to a commercial alloy and hence the effect of impurity segregation should be taken into account (not only Cr, but also other minor alloying elements). The segregation of solute atoms tends to lower the energy of each individual GB, which is the result of the interaction of the strain field around the solute atom and the strain field near the boundary. In addition, segregation reduces the energy difference between the relatively ordered and disordered GBs. It is commonly accepted that the segregation tendency increases with increasing disorderness of the boundary since they have a higher dislocation density and hence a higher concentration of solute atoms segregated at dislocations [36]. The segregation of solute atoms in turn lowers the GB energy where segregation occurs. As a result, the segregation effect will lead to a decreasing difference between the energy of ordered and disordered GBs.

Another possible explanation for the smaller variation range of the data-sets of this study is that the GB energy calculated here was at a much higher temperature. The influence of temperature on the variation in GB diffusivity and GB energy as a function of disorientation angle from relatively ordered (small angle GBs and CSL GBs) to disordered GBs (large angle non-special GBs) is thus discussed as follows:

Recall that the GB diffusion coefficients calculated in this study are those of Cr in the GBs of the alloy, which was the product of the segregation coefficient (s) and the GB diffusion coefficient (D_{GB}). Both the segregation coefficient and the GB diffusivity terms contain an exponential term including activation energy and temperature. Thus, the activation energy of the diffusion coefficient of Cr in the alloy GBs (Q_{GB}) is the sum of the actual diffusion activation energy (H_{GB}) and the segregation enthalpy (H_s) as expressed in Equation (5):

$$Q_{GB} = H_{GB} + H_s \tag{5}$$

The activation energy of diffusion for the more ordered GBs is larger than that of the disordered GBs. This should lead to a decreasing diffusivity difference between ordered and disordered GBs as temperature increases. On the other hand, it was reported that the segregation enthalpy was much smaller than the actual diffusion activation energy [37–39]. In addition, it was reported that Cr has a low tendency to segregate at Fe GBs [23]. Thus the contribution of the effect of segregation should be relatively small comparing to the effect of diffusion activation energy. Hence, taking both of the above factors into account, an increase in the temperature should result in decreasing diffusivity difference between ordered and disordered GBs.

As for the GB energy, there are two main factors contributing to the temperature effect. The first one is the effect of the entropy term in the GB energy expression Equation (6):

$$G = H - TS, \tag{6}$$

where G is the GB Gibbs free energy; H is the GB enthalpy; T is the temperature; and S is the GB entropy. The relatively ordered boundaries should have lower values for the entropy term than the disordered boundaries. As the temperature rises, the entropy term becomes increasingly important and as a result, the energy difference between ordered and disordered boundaries should decrease according to Equation (6).

The second factor contributing to the temperature effect is the GB segregation effect. As addressed above, the segregation of solute atoms tends to lower the energy of each individual GB and reduce the energy difference between relatively ordered and disordered GBs. As temperature rises, some solute atoms disperse in the adjoining lattice [35]. In addition, it has been reported that the GB segregation anisotropy (the difference in the amount of segregated solute atoms between ordered and disordered GBs) decreases as temperature increases [40]. This should result in an increasing energy difference between the ordered and disordered GBs, which will counteract the effect of the entropy term. However, without further data regarding segregation, which of the two factors (entropy term or segregation effect) is predominant is yet to be determined.

Erb et al. measured the GB energy in Cu (99.999%) as a function of temperature [41]. They concluded that the GB entropy effects resulted in a reduction of the number and width of the cusps in the energy misorientation curve with increasing temperatures. This agrees with this study. Miura et al. measured the temperature dependence of the energy of the [1 1 0] symmetrical tilt GBs in Cu-0.06 wt % Si alloy [42]. Their results showed that as the temperature decreased, the CSL energy cusps became wider and shallower. This observation is opposite to the result of this study. However, both of these studies were conducted in nearly pure material and the segregation effect was not taken into account. Shivindlerman analysed the experimental data by other workers and observed that some energy cusps vanished with increasing temperature, which is in agreement with this study [43]. Their conclusion was that some of the special boundaries might have transformed into non-special boundaries below the melting temperature.

A final comment on the method used to collect the volumetric data of the oxide ridges:

While being able to collect a reasonably large amount of quantitative data via AFM, it is still quite a tedious process. There are other techniques (not available to us) that can collect the same type of data with much ease, which in general usually involve imaging and a subsequent computerised three-dimensional reconstruction from the images.

Following the general methodology presented in this study, if the volumetric data of the oxide ridges can be collected from a relatively large surface, GB diffusivity and GB energy data can hence be extracted that are statistically meaningful. Even though this method may still fall into the so-called two-dimensional 'GB misorientation approach', the data can serve as the basis for a quick approximate evaluation of GB-related properties and performance.

4. Summary

The size of the oxide ridges on the post oxidation surface of Fe-22 wt % Cr alloy emerged along GBs during transient stage oxidation at 800 °C in dry air was measured by AFM. The ridge size data were used to calculate GB diffusivity and GB energy to make better comparison with the data available in the literature. The conclusions drawn from this work are summarised as follows:

- The calculated GB diffusivity was slightly smaller than the commonly seen values of Cr in α-Fe at 800 °C reported in the literature, but still within the range.
- The absolute value of the calculated GB energy was also smaller than the value in the literature. Also, the data-sets obtained from this study showed much less spread than the data-set in literature.

- This less spread of the data-sets from this study is attributed to the effect of segregation and the much higher temperature condition (1073 K) in this study compared to the ground state (0 K) conditions used in the literature. As temperature increases the variation range of the GB diffusivity as function of disorientation angle decreases while whether the variation range of the GB energy should increase or decrease depends on two conflicting factors: entropy term and segregation effect. Further study is needed to determine which of the factors is predominant.

Acknowledgement

The authors acknowledge use of the Materials Characterization Facility at Carnegie Mellon University supported by [grant number MCF-677785]. Also, the National Natural Science Foundation of China [grant number 51501231] is acknowledged. The authors would like to thank Professor Gregory S. Rohrer of the Department of Materials Science and Engineering at Carnegie Mellon University for helpful discussions. We also thank Yang Wang, a former graduate student in the Department of Mechanical Engineering at Carnegie Mellon University for the help in the programming for data processing.

Disclosure statement

No potential conflict of interest was reported by the authors.

Funding

The work was supported by the Materials Characterization Facility at Carnegie Mellon University supported by [grant number MCF-677785]. Also, the National Natural Science Foundation of China [grant number 51501231]

ORCID

Jingxi Zhu http://orcid.org/0000-0002-0019-0647

References

[1] J. Zhu, L.M.F. Diaz, G.R. Holcomb, P.D. Jablonski, C.J. Cowen, D.E. Laughlin, D. Alman, and S. Sridhar, *On the relation between oxide ridge evolution and alloy surface grain boundary disorientation in Fe-22wt%Cr alloys*, J. Electrochem. Soc. 157 (2010), pp. B655–B664.
[2] D. Young, *High Temperature Oxidation and Corrosion of Metals*, 1st ed., Elsevier, Oxford, 2008.
[3] I. Kaur, Y. Mishin, and W. Gust, *Fundamentals of Grain and Interphase Boundary Diffusion*, 3rd ed., John Wiley & Sons, New York, 1995.
[4] N. Birks, G.H. Meier, and F.S. Pettit, *Introduction to the High Temperature Oxidation of Metals*, 2nd ed., Cambridge University Press, Cambridge, 2006.
[5] T. Horita, H. Kishimoto, K. Yamaji, Y. Xiong, N. Sakai, M.E. Brito, and H. Yokokawa, *Effect of grain boundaries on the formation of oxide scale in Fe–Cr alloy for SOFCs*, Solid State Ionics 179 (2008), pp. 1320–1324.
[6] C. Thorning and S. Sridhar, *Grain boundary ridge formation during initial high temperature oxidation of Mn/Al TRIP steel*, Philos. Mag. 87 (2007), p. 3479.
[7] B. Chattopadhyay and G.C. Wood, *The transient oxidation of alloys*, Oxid. Met. 2 (1970), pp. 373–399.

[8] B. Chattopadhyay and G.C. Wood, The transient oxidation of Fe–Cr and Ni–Cr alloys, J. Electrochem. Soc. 117 (1970), pp. 1163–1171.
[9] A.P. Sutton and R.W. Balluffi, *On the geometric criteria for low interfacial energy*, Acta Metall. 35 (1987), pp. 2177–2201.
[10] R.W. Balluffi, *Grain boundary diffusion mechanisms in metals*, Metall. Trans. A 13A (1982), pp. 1982–2069.
[11] H. Gleiter, *The structure and properties of high-angle grain boundaries in metals*, Phys. Status Solidi A 45 (1971), p. 9.
[12] D. Turnbull and R.E. Hoffman, *The effect of relative crystal and boundary orientations on grain boundary diffusion rates*, Acta Metall. 2 (1954), p. 419.
[13] A.N. Aleshin, VYu Aristov, B.S. Bokshtein, and L.S. Shvindlerman, *Kinetic properties of <1 1 1> tilt boundaries in aluminium*, Phys. Status Solidi A 45 (1978), p. 359.
[14] N. Aleshin, B.S. Bokshtein, and L.S. Shvindlerman, *Diffusion of zinc along 1 0 0 tilt boundaries in aluminium*, Sov. Phys. Solid State 19 (1977), pp. 2051–2054.
[15] B. Straumal, B.S. Bokshtein, L.M. Klinger, and L.S. Shvindlerman, *Indium diffusion on single torsion interphase boundaries in (0 0 1) Sn–Ge*, Fizika Tverdogo Tela 24 (1982), pp. 1317–1320.
[16] E. Budke, C. Herzig, S. Prokofjev, and L.S. Shvindlerman, *Orientation dependence of Au and Cu diffusion along symmetric [0 0 1] tilt grain boundaries in Cu*, Mater. Sci. Forum (1966), pp. 207–209.
[17] V.T. Borisov, V.M. Golikov, and G.V. Scherbedinskiy, *Relation between diffusion coefficients and grain boundary energy*, Phys. Met. Metall. 17 (1964), pp. 881–885.
[18] P. Eaton and P. West, *Atomic Force Microscopy*, Oxford University Express, Oxford, 2010.
[19] S. Yumoto and N. Ookubo, *Fast imaging method combining cantilever and feedback signals in contact-mode atomic force microscopy*, Appl. Phys. A 69 (1999), pp. 51–54.
[20] I. Saeke, H. Konno, and R. Furuichi, *Initial oxidation of type 430 stainless steels with 0.09–0.9 Mn in O_2–N_2 atmosphere at 1273 K*, Corros. Sci. 38 (1996), pp. 1595–1612.
[21] G.S. Rohrer, *Structure and bonding in crystalline materials*, Cambridge University Press, Cambridge, 2004.
[22] J.C. Fisher, *Calculation of diffusion penetration curves for surface and grain boundary diffusion*, J. Appl. Phys. 22 (1951), pp. 74–77.
[23] H.A. Murdoch and C.A. Schuh, *Estimation of grain boundary segregation enthalpy and its role in stable nanocrsystalline alloy design*, J. Mater. Res. 28 (2013), pp. 2154–2163.
[24] A.M. Huntz, M. Aucouturier, and P. Lacombe, *Mesure des coefficients de diffusion en volume et intergranulaire du chrome radioactive dans le fer α* [Measurement of the volume and intergranular diffusion coefficients of radioactive chromium in alpha-iron], C. R. Acad. Sci. C265 (1967), p. 554.
[25] P. Guiraldenq and P. Poyet, *Influence of nickel on the volume and intercrsystalline diffusion in austenitic Fe–Cr–Ni alloys – Grain boundary energy evolution as a function of composition*, Mem. Sci. Rev. Metall. 70 (1973), pp. 715–723.
[26] P. Guiraldenq, *Diffusion intergranulaire et energie des joints de grains* [Grain boundary diffusion and energy], J. Phys. C. 36 (1975), pp. 201–211.
[27] A.M. Huntz, P. Guiraldenq, M. Aucouturier, and P. Lacombe, *Relation between the diffusion of radioactive Fe and Cr in Fe–Cr alloys with 0–15% Cr and their α/γ transformation*, Mem. Sci. Rev. Met. 66 (1969), pp. 85–104.
[28] Zs. Tokei, K. Hennesen, H. Viefhaus, and H. Grabke, *Diffusion of chromium in ferritic and austenitic 9–20 wt% chromium steels*, Mater. Sci. Technol. 16 (2000), pp. 1129–1138.
[29] J. Čermák, J. Růžičková, and A. Pokorná, *Low-temperature tracer diffusion of chromium in Fe–Cr ferritic alloys*, Scr. Mater. 35 (1996), pp. 411–416.
[30] R.A. Perkins, R.A. Padgett Jr, and N.K. Tunali, *Tracer diffusion of 59Fe and 51Cr in Fe-17 wt pct-12 wt pct Ni austenitic alloy*, Metall. Trans. 4 (1973), pp. 2535–2540.
[31] W. Assassa and P. Guiraldenq, *Influence du carbone sur les cinetiques de diffusion en volume et aux joints des elements de base dune solution solide austenitique Fe–Cr–Ni* [Influence of C on the kinetics of diffusion in bulk and at grain boundaries of the base elements of an Fe-Cr-Ni austenitic stainless steel], Metaux-Corrosion-Industrie 621 (1977), pp. 170–181.

[32] R.W. Balluffi, S.M. Allen, and W.C. Carter, *Kinetics of Materials*, John Wiley & Sons, New York, 2005.
[33] C. Minkwitz, C. Herzig, E. Rabkin, and W. Gust, *The inclination dependence of gold tracer diffusion along a Σ3 twin grain boundary in copper*, Acta Mater. 47 (1999), pp. 1231–1239.
[34] S. Ratanaphan, D.L. Olmsted, V.V. Bulatov, E.A. Holm, A.D. Rollett, and G.S. Rohrer, *Grain boundary energies in body-centered cubic metals*, Acta Mater. 88 (2015), pp. 346–354.
[35] D. Gupta, Influence of solute Segregation on grain-boundary energy and self-diffusion, Metall. Trans. A 8 (1977), pp. 1431–1438.
[36] P. Lejcek and S. Hofmann, *Thermodynamics and structural aspects of grain boundary segregation*, Solid State Mater. Sci. 20 (1995), pp. 1–85.
[37] E. Budke, T. Surholt, S.T.L.S. Prokofjev, L.S. Shivindlerman, and C. Herzig, *Tracer diffusion of Au and Cu in a series of near Σ = 5 (3 1 0) [0 0 1] symmetrical Cu tilt grain boundaries*, Acta Mater. 47 (1999), pp. 385–395.
[38] S.V. Divinski and H. Edelhoff, *Diffusion and segregation of silver in copper Σ5 (3 1 0) grain boundary*, Phys. Rev. B 85 (2012), pp. 144104.
[39] T. Frolov, S.V. Divinski, M. Asta, and Y. Mishin, Effect of interface phase transformations on diffusion and segregation in high-angle grain boundaries, Phys. Rev. Lett. 110 (2013), p. 255502.
[40] P. Lejcek, J. Adamek, and S. Hofmann, *Anistropy of grain boundary segregation in Σ = 5 bicrystals of α-iron*, Surf. Sci. 264 (1992), pp. 449–454.
[41] U. Erb and H. Gleiter, *The effect of temperature on the energy and structure of grain boundaries*, Scr. Metall. 13 (1979), pp. 61–64.
[42] H. Miura, M. Kato, and T. Mori, *Temperature dependence of the energy of Cu [1 1 0] symmetrical tilt grain boundaries*, J. Mater. Sci. Lett. 13 (1994), pp. 46–48.
[43] L.S. Shvinlerman and R.B. Straumal, *Regions of existence of special and non-special grain boundaries*, Acta Metall. 33 (1985), pp. 1735–1749.